Turkish Journal of Chemistry
http://journals.tubitak.gov.tr/chem/
Research Article

Turk J Chem
(2015) 39: 317 – 333

doi:10.3906/kim-1409-56

Improvement of solubility of celecoxib by inclusion in MCM-41 mesoporous silica: drug loading and release

Şahika GÜNAYDIN[1], **Ayşen YILMAZ**[1,2,*]
[1]Department of Chemistry, Middle East Technical University, Ankara, Turkey
[2]Department of Micro and Nanotechnology, Middle East Technical University, Ankara, Turkey

Received: 22.09.2014 • **Accepted/Published Online:** 04.12.2014 • **Printed:** 30.04.2015

Abstract: Celecoxib is a poorly water-soluble nonsteroidal anti-inflammatory drug. Here we report four ordered mesoporous silica MCM-41 supports with different particle size, pore volume, and surface properties to investigate their loading capacity with celecoxib and their release abilities. Spherical MCM-41 mesoporous supports less than 50 nm in diameter were prepared and to compare the effect of the template removal process on morphology of samples, acid extraction and calcination methods were used. Moreover, nearly 500 nm sized rod-shaped MCM-41 mesoporous silica was obtained by changing the template concentration in preparation. Boron doping was performed to determine the effect of a heteroatom on the surface of mesoporous silica and adsorbance of drug molecules and release. In order to investigate the effect of polarity of solvent during drug loading, two different solvents were used: ethanol as polar solvent and hexane as nonpolar solvent. All bare and drug-loaded samples' physicochemical characterizations were performed. The release experiments were conducted in phosphate buffer solution of pH 7.4 at 37 °C. Celecoxib solubility was highly improved compared to the pure drug. The morphology and surface property differences of MCM-41 and the solvent effect in adsorption of celecoxib have been discussed, including its delivery.

Key words: Poorly water-soluble drugs, MCM-41, drug delivery system, borosilicate, celecoxib

1. Introduction

The synthesis of mesoporous silica materials (M41S family) by surfactant-templated sol-gel method was first reported in the early 1990s.[1,2] Since then, these materials have attracted the attention of many researchers because of their unique properties: highly ordered structure, uniform pore size, and high hydrothermal stability. Various synthesis methods lead to different morphologies; for example, spherical, fibrous, or vesicle particles can be produced by changing the surfactant to silicate ratio in solution.[3] The large internal surface of these materials can be functionalized with organic molecules by co-condensation or postgrafting method to extend their application area.[4,5] In comparison, the latter is much more advantageous in order to obtain hydrothermally stable and selectively functionalized materials.[6] There are many ways to remove template from silica; only two of them were used in preparation of samples in this report: calcination by heating at nearly 500 °C for at least 5 h or acid extraction, which involves refluxing the product in an alcohol and acid mixture for several hours to prevent agglomeration of particles due to heat.[7] In order to reduce the particle size of mesoporous silica (common synthesis methods lead to the formation of particles with diameter of 500 nm to micrometers), very dilute solutions of template are prepared at the beginning of synthesis.[8]

*Correspondence: ayseny@metu.edu.tr

Recently, many scientists have been using silica-based mesoporous materials in biomedical studies such as imaging or disease treatment.[9–11] As we focused on in this study, one of the promising usage areas of mesoporous materials is drug delivery systems. Since the MCM-41 (Mobil Composition of Matter No. 41, having one-dimensional ordered hexagonal channels, large surface area, narrow pore size distribution, and stable mesoporous structure) was used as a carrier in drug delivery systems in 2001, mesoporous silica materials have attracted lots of attention as drug carriers and controlled-release systems. While the high pore volume of the mesoporous silica materials enables them to hold the required amount of drug molecules, their ordered pore network allows controlled release of the drug in the targeted area.[12] During the delivery of the drug in the body fluid, premature degradation of drug molecules can be prevented. These unique properties of mesoporous particles make them perfect candidates as carriers in drug delivery systems.[13]

Although there are different ways of drug intake, oral administration is the most desired one, because it is simple and painless and the dosage is easily controlled. To deliver a drug molecule to the targeted area in the body in an effective way, bioavailability of the drug is the most important concern. For a drug molecule to be called bioavaliable, it should have three important features: solubility, permeability, and stability. However, it has been reported that 40% of recently developed pharmaceutical agents are poorly water soluble or insoluble. Therefore, enhancing the solubility of a hydrophobic drug is an important aspect in developing and achieving optimum absorption of a drug molecule.[14–16]

The physical form of the drug, composition of the solvent medium, and environmental conditions can be counted as factors affecting the solubilization of hydrophobic drugs. Size of the drug molecule is the most important factor influencing solubility. As the size of the drug molecule decreases, its surface area increases. With the increasing surface area, drug molecules can interact with the solvent easily. When the temperature of the system is increased, solution that contains drug molecules absorbs energy and its solubility increases as well. The solubility of the drug is increased when molecules have lower molecular weight and lower molecular size because larger molecules are more difficult to surround with solvent molecules. Polarity is the other factor affecting the solubility of hydrophobic drugs. The polar drug molecules have a positively and a negatively charged end. If the solvent molecule is also polar then positive ends of solvent molecules will attract negative ends of solute molecules. Dipole–dipole interaction enhances the solubility of hydrophobic drug molecules.[17]

Celecoxib is chemically designated as 4-[5-(4-methylphenyl)-3-trifluoromethyl)-1H-pyrazol-1-yl] benzene sulfonamide, with the empirical formula $C_{17}H_{14}F_3N_7O_2S$ and molecular weight of 381.373 g/mol (Figure 1). It is a nonsteroidal anti-inflammatory drug (NSAID) and is generally used in the treatment of pain and inflammation. Celecoxib is hydrophobic; at pH 7 and 40 °C, its solubility in water is 3–7 μg/mL. Due to its poor water solubility and high lipophilicity, it is classified as a class II drug according to the Biopharmaceutics Classification Scheme. It is also a weak acid with pKa $\approx$ 11.[18] Celecoxib selectively inhibits the cyclooxygenase-2 enzyme. Cyclooxygenase (COX) is an enzyme that is responsible for converting arachidonic acid to the prostanoids that result in pain and inflammation. There are two different types of COX: COX-1 and COX-2. While inhibition of COX-1 is undesirable, inhibition of COX-2 is desirable. Traditional NSAIDs are nonselective and inhibit both COX enzymes. However, inhibition of COX-1 can lead to NSAID toxicity and cause mucosal damage, ulceration, and ulcer complications in the gastrointestinal tract. Celecoxib binds to the hydrophilic side pocket region of COX-2 with its polar sulfonamide side chain; this selectivity allows celecoxib to reduce inflammation and pain. It also minimizes adverse gastrointestinal effects that are common with traditional nonselective NSAIDs. Celecoxib is safer than traditional NSAIDs because of its selectivity.[19,20]

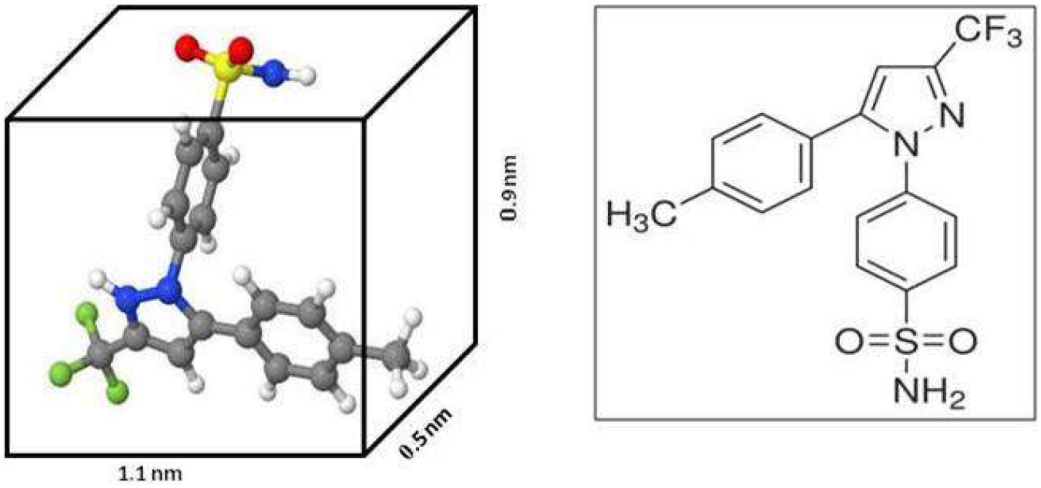

Figure 1. Chemical structure of celecoxib.

This report is the first research to investigate the loading and release properties of celecoxib in MCM-41 silica support. There are manuscripts in the literature about improvement of solubility of celecoxib deposited in several silica supports. For example, with the purpose of enhancing the solubility and oral bioavailability of celecoxib, Tan et al.[21] investigated silica-lipid hybrid microcapsules that were composed of medium-chain triglycerides, lecithin, and silica nanoparticles to encapsulate celecoxib molecules. They observed an increased release rate and better dissolution of celecoxib. In addition, they increased the stability of the drug by this encapsulation technique. In other research, Zhao et al.[22] used fibrous ordered mesoporous carbon as drug carrier due to its high surface area, large pore volume, and strong absorption ability. It was reported that 1 g of mesoporous carbon was loaded with 0.599 g of celecoxib. Furthermore, their samples showed a faster release rate and caused no damage to gastric mucosa. By using ethanol as a solvent in the loading process, they managed to change the crystalline state of the celecoxib to noncrystalline and enhanced its bioavailability. In addition, Wang and colleagues loaded 20%–30% (by wt) celecoxib into 3D face-centered mesoporous silica with higher pore size (16.0, 6.9, and 3.7 nm) by solvent deposition method in methanol and observed two-stage release in an in vitro drug release experiment: burst release (0–10 min) and prolonged release (10–60 min). The cumulative release of celecoxib from support was 63% (16.0 nm), 46% (6.9 nm), and 58% (3.7 nm) in first 30 min; the pore size values written in parentheses prove uniform drug loading and pore size, both very important in enhancing the dissolution properties of poorly water-soluble drugs.[23]

In the present study, firstly our aim was to synthesize MCM-41 type silica particles with different particle sizes and surface properties and use them as support materials to deposit celecoxib and then examine their drug release behavior in aqueous solution. According to TEM results, MCM-41-1 and MCM-41-2 labeled particles with diameter less than 100 nm and MCM-41-3 labeled particles with diameter about 500 nm were prepared in order to compare the morphology effect. In addition, to examine the effect of boron doping on the silica network, boron added MCM-41 particles were prepared and labeled as B-MCM-41; they have particles larger than 500 nm. With the purpose of observing the effect of solvent on the loading efficiency of celecoxib, two different solvents were used: ethanol and hexane. In this way, we wanted to enhance the bioavailability of this hydrophobic drug.

2. Results and discussion

2.1. Characterization

Small angle (as inset) and wide angle powder XRD patterns of four different support materials, mesoporous MCM-41 and MCM-41 loaded with drug in ethanol and hexane solvent, can be seen in Figure 2A-2D. In the small angle powder XRD pattern of bare MCM-41 nanoparticles exhibit a very intense diffraction peak between $2\theta = 2$ and 2.5° and two different peaks of lower intensity at $2\theta = 4$ and 5°. All the sample patterns show these characteristic diffraction peaks of a 2-D hexagonal lattice structure. XRD patterns of MCM-41 materials are hexagonally ordered with the space group P6mm. This indicates good ordering of the hexagonal mesophase of the samples. The diffraction peaks were assigned to the planes as (100), (110), and (200), and the unit cell parameter, a, was calculated by using $a = 2d/\sqrt{3}$. After drug loading, all the materials demonstrated similar XRD patterns to those before loading, even though the major diffraction peak intensities had decreased slightly. This is normally caused by the decrease in the scattering intensity contrast between the walls of the mesoporous material and the channel pores when organic substances are incorporated onto the pore surface.[24] It means that the ordered structure of MCM-41 supports was preserved after celecoxib loading. Compared to MCM-41, intensities of XRD peaks of drug-loaded silica nanoparticles are lower. According to wide angle XRD patterns of MCM-41 samples, it can be recognized that the broad peak between 20 and 30° was preserved after celecoxib loading in ethanol. The only difference between the XRD patterns of MCM-41 and drug-loaded MCM-41 was the presences of the sharp peaks at 20°, which are the diffraction peaks of celecoxib. While the decrease in the intensities of the characteristic peaks in small angle XRD patterns can be explained by the loading of celecoxib into the pores of MCM-41 samples, the presence of the peaks at 20° can be explained by the adsorption of celecoxib into the outer surface of the samples in crystalline form. When the small angle XRD patterns of MCM-41 samples drug loaded in hexane were investigated, decreases in the intensities of the characteristic peaks of the 2-D hexagonal lattice structure compared to bare samples were seen again. Celecoxib drug molecules probably stayed in crystalline state during the process of drug loading in hexane and attached to the outer surface of the samples, which can be observed in the wide angle XRD patterns of samples. The patterns of MCM-41 in the wide angle part of the drug loaded in hexane showed almost all of the peaks of celecoxib. The crystalline state of the drug molecules was probably maintained and adsorbed on the surface of the carrier in hexane. Due to these drug molecules in the crystalline state attached to the surface of the MCM-41, all of the characteristic peaks of celecoxib were seen in the XRD pattern of drug loaded MCM-41 samples. Thermogravimetric and elemental analyses were performed to evaluate the percentages of celecoxib loaded (Table). The elemental analysis data were collected according to carbon content of samples, which has carbon source as the only drug molecules. The weight loss in thermogravimetric analyses and carbon content of samples were used to quantify the amount of celecoxib in mesoporous silica supports. For each sample, the quantities of drug calculated by thermogravimetric and elemental analyses are in accordance.

The purpose of Brunauer–Emmett–Teller (BET) analysis in this study was to observe the effect of celecoxib loading on the surface area and pore size changes. Figures 3A-3D depict the BET isotherms of MCM-41 samples loaded with celecoxib in ethanol and hexane. All the MCM-41 samples exhibited type IV BET isotherms, showing the presence of a mesoporous characteristic. For the type IV isotherm, in low relative pressures, gas fills the mesopores until the sharp increase at around $P/P_0 = 0.3$. The monolayer adsorption followed by multilayer formation of nitrogen occurs in the flatter region between the relative pressure at 0.3 and 0.9. After that point, nitrogen starts to be condensed in the capillary pores of porous material at pressures below the saturation pressure. A sharp increase at the relative pressure about 0.9 is indicated as narrow pore

Table. Unit cell parameter, pore volume, pore size, surface area, zeta potential, drug loading, and release values of samples.

	MCM-41-1			MCM-41-2			MCM-41-3			B-MCM-41		
	Bare	CLX_{eth}	CLX_{hex}	Bare	CLX_{eth}	CLX_{hex}	Bare	CLX_{eth}	CLX_{hex}	Bare	CLX_{eth}	CLX_{hex}
d (Å)	36.2	39.4	36.8	31.9	34.7	34.2	35.2	36.9	36.3	34.5	35.9	37.4
a (Å)	41.8	45.5	42.5	36.8	40.1	39.5	40.6	42.6	41.9	39.8	41.5	43.2
Pore volume (cm^3/g)	1.146	1.124	0.488	2.087	1.451	0.557	0.125	0.0917	0.0910	1.203	0.6625	0.2261
Pore diameter (nm)	1.438	2.487	1.952	2.459	2.201	2.204	1.439	2.522	3.125	2.443	2.463	2.185
Surface area (m^2/g)	763.9	457.5	114.5	1020	704.1	336.3	320.0	127.1	39.362	1095	816.6	243.8
Zeta potential (mV)	–6.74	-	-	–2.94	-	-	–2.55	-	-	–31.7	-	-
CLX loading - elemental analysis	-	26.40%	-	-	18.98%	-	-	19.48%	-	-	16.21%	-
CLX loading -UV analysis	-	25.95%	29.51%	-	20.95%	22.92%	-	25.21%	25.58%	-	17.57%	23.89%
CLX loading - TGA	-	25.13%	-	-	17.99%	-	-	21.33%	-	-	17.96%	-
CLX release - UV analysis	-	72.83%	60.11%	-	75.82%	64.44%	-	62.48%	59.12%	-	86.78%	66.22%

size distribution and highly ordered mesostructure.[25,26] As can be seen from the BET isotherms of MCM-41 samples, all the adsorption–desorption processes are reversible. Hysteresis loops are narrow in this analysis, which can be explained by the uniformity of pores and channels in MCM-41 samples. These trends in results can be seen in the samples loaded with drug in hexane, explained by the stability of pores. After the celecoxib loading process, pores preserved their uniformity and did not degrade.[26] According to Ravikovitch et al.,[27] the dimension of the hysteresis loop decreases with the decrease in pore size. According to the results, pores of MCM-41 samples were 1.4–3.1 nm in diameter and the hysteresis loop may be narrow.

Exceptionally, MCM-41-3 has a relatively broadened hysteresis loop that is irreversible. This sample probably does not have the same uniformity as the other samples have. In order to analyze the porosity and surface area of MCM-41 samples before and after celecoxib loading in detail, the Table shows the pore volume, pore diameter, and surface area data. When the pore diameters were analyzed, a decrease in data with drug loading was seen, which indicates successful grafting in the internal surface of the MCM-41 particles. However, MCM-41-2 and MCM-41-3 samples showed an increase in hexane, while pore diameters of MCM-41-1, MCM-41-3, and B-MCM-41 increased in ethanol. For example, for samples loaded in hexane, although this increase was negligible in MCM-41-2 samples, pore diameter of MCM-41-3 particles increased to 3.125 nm from 1.439 nm after celecoxib loading. This may be because of the adsorption of drug molecules to the outer surface of the MCM-41-3 sample. However, according to Kruk et al.[25] and many other studies aimed to investigate the exact pore diameter of porous materials, data given in N_2 adsorption–desorption results are core diameter and do not reflect the actual pore size, because they examine the inner free space in the pore that is not filled with adsorbate during the adsorption process or emptied by capillary evaporation during the desorption process. This means N_2 adsorption–desorption analysis just concerns free space in the pores. In contrast to assumptions

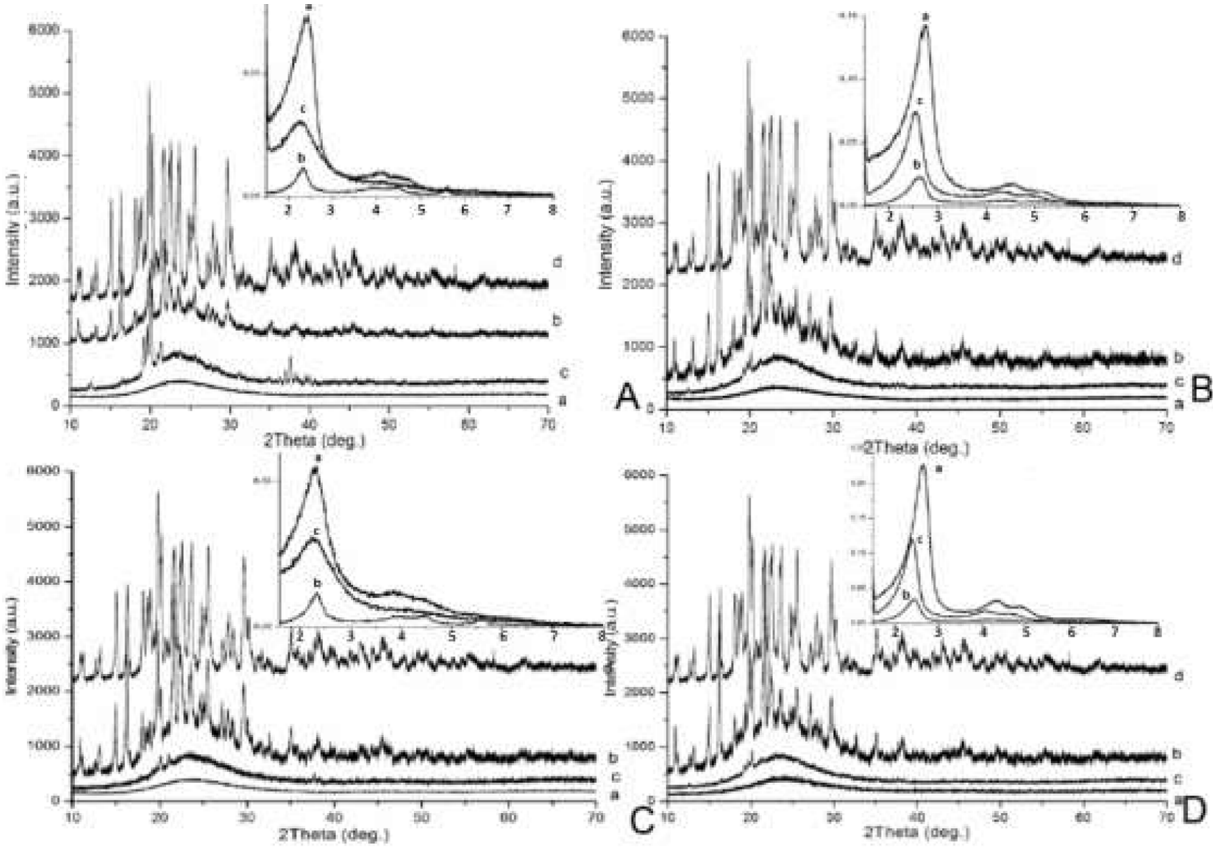

Figure 2. XRD patterns of mesoporous silica supports and celecoxib-loaded materials in ethanol and hexane A) MCM-41-1(a) MCM41-1, b) MCM41-1@Clx$_{hex}$ (celecoxib loaded into MCM41 in hexane), c) MCM41-1@Clxeth (celecoxib loaded into MCM41 in ethanol solvent), d) Celebrex, B) MCM-41-2, (a) MCM41-2, b) MCM41-2@Clx$_{hex}$ (celecoxib loaded into MCM41 in hexane), c) MCM41-2@Clx$_{eth}$ (celecoxib loaded into MCM41 in ethanol), d) Celebrex, C) MCM-41-3, (a) MCM41-3, b) MCM41-3@Clx$_{hex}$ (celecoxib loaded into MCM41 in hexane), c) MCM41-3@Clx$_{eth}$ (celecoxib loaded into MCM41 in ethanol), d) Celebrex, D) B-MCM-41, (a) B-MCM41, b) B-MCM41@Clx$_{hex}$ (celecoxib loaded into MCM41 in hexane), c) B-MCM41@Clx$_{eth}$ (celecoxib loaded into MCM41 in ethanol), d) Celebrex.

made during this analysis, Kaminsky et al.[28] state that each pore is filled with adsorbate discontinuously and incompletely. Due to these results, it is possible to see some deviations in data reflecting pore diameters and it is not that easy to make an observation by this way. Nevertheless, the N_2 adsorption–desorption process is still the most practical way.

The Barrett–Joyner–Halenda (BJH) method is used to investigate the pore size distribution of porous materials. Although there may be some deviations in the pore diameter data, in order to make an observation about the pore size distribution, it is the easiest and most practical way. Figure 3's insets show the pore size distribution of MCM-41 and samples loaded with celecoxib in ethanol and hexane. According to the pore size distribution calculated by the BJH method, all the MCM-41 samples show a narrow pore size distribution in the range of 2–3 nm. Although there is still a narrow pore size distribution, homogeneity decreased after celecoxib loading.

Zeta potential measurements aim to obtain information about the surface properties of MCM-41 silica particles by using electric potential. They give information about the net surface charge of the particles. For

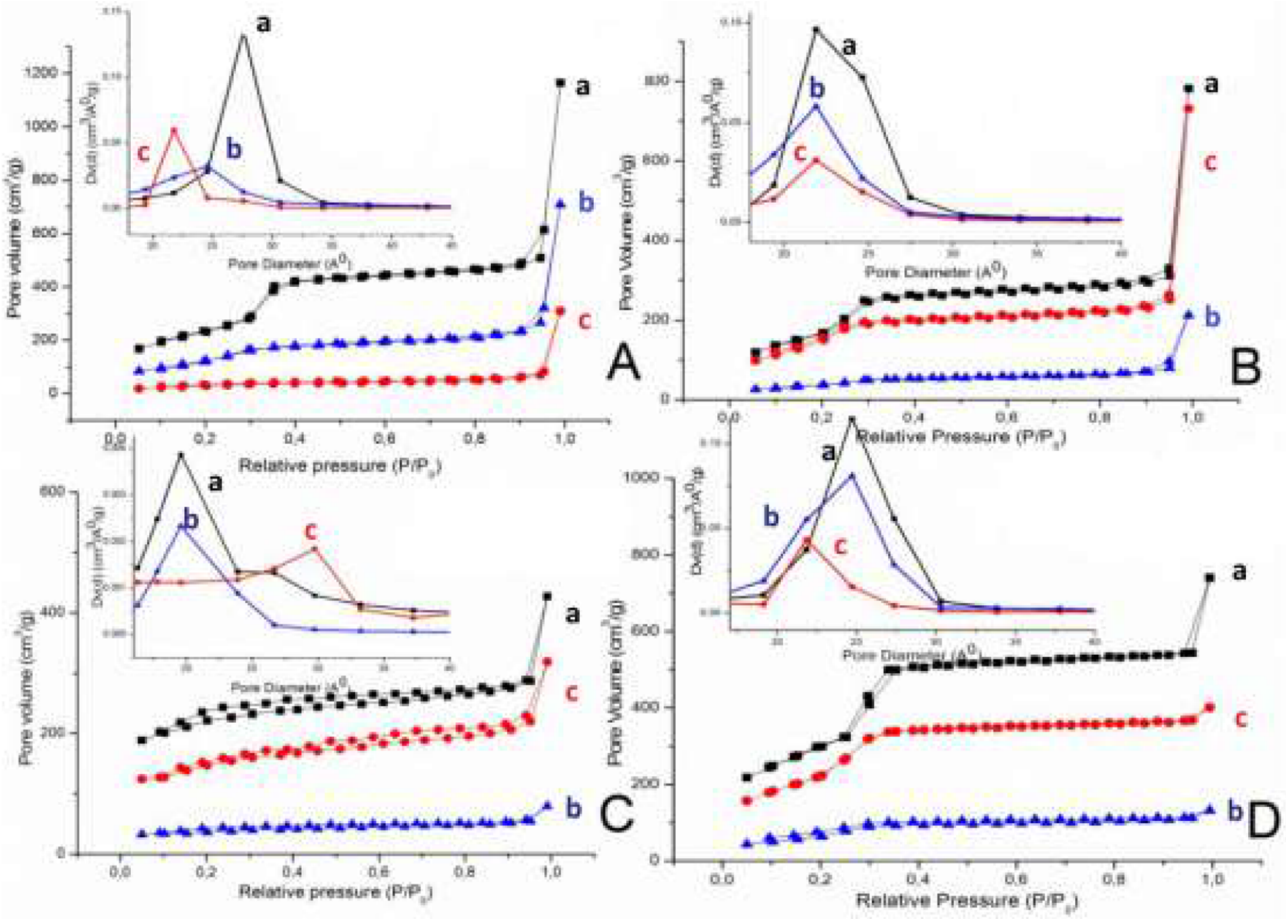

Figure 3. N_2 adsorption and desorption isotherms and pore size distributions of synthesized mesoporous materials. A) MCM-41-1(a) MCM41-1, b) MCM41-1@Clx$_{hex}$ (celecoxib loaded into MCM41 in hexane), c) MCM41-1@Clx$_{eth}$ (celecoxib loaded into MCM41 in ethanol), B) MCM-41-2, (a) MCM41-2, b) MCM41-2@Clx$_{hex}$ (celecoxib loaded into MCM41 in hexane), c) MCM41-2@Clx$_{eth}$ (celecoxib loaded into MCM41 in ethanol), C) MCM-41-3, (a) MCM41-3, b) MCM41-3@Clx$_{hex}$ (celecoxib loaded into MCM41 in hexane), c) MCM41-3@Clx$_{eth}$ (celecoxib loaded into MCM41 in ethanol), D) B-MCM-41, (a) B-MCM41, b) B-MCM41@Clx$_{hex}$ (celecoxib loaded into MCM41 in hexane), c) B-MCM41@Clx$_{eth}$ (celecoxib loaded into MCM41 in ethanol).

this purpose, a 0.001-g MCM-41 sample was suspended in 50 mL of deionized water. The Table shows the zeta potential values of MCM-41 silica particles. Although there are small differences between them, all MCM-41 samples exhibit a negative surface charge. This is because of the negatively charged silanol groups on the surface of the MCM-41 samples.[29] However, the surface of borosilicate is highly negative with a zeta potential of –31.7 mV. This value is more negative than the other zeta potentials of MCM-41 samples. This may be due to the high electronegativity of boron in the borosilicate.

Thermogravimetric analysis is a method of thermal analysis in which the sample is heated to elevated temperature and the weight loss is monitored as a function of increasing temperature. TGA analysis can provide information about many physical and chemical phenomena such as second-order transition, sublimation, absorption, adsorption, chemisorption, dehydration, decomposition, oxidative degradation, and solid-state reactions.[30] Loss in weight is mainly related to the adsorbed H_2O and formation of oxides and gases such as CO_2, NH_3, N_2,

NO_x, and SO_y at temperatures below 200 °C. Weight loss due to celecoxib occurred between the temperatures of 200 °C and 600 °C. Therefore, calculations of celecoxib loaded to MCM-41 silica nanoparticles were done according to the weight loss in this temperature range. In Figure 4, % weight loss of MCM-41 nanoparticles and MCM-41 nanoparticles loaded with celecoxib in ethanol can be seen. In the Table, there are data calculated for celecoxib loaded onto carrier in ethanol according to UV analysis and TGA analysis. As can be seen, the values are really close to each other. This confirms the amount the celecoxib loaded onto MCM-41 silica nanoparticles. It can be seen that weight loss of the MCM-41 nanoparticles that are not loaded with celecoxib are negligible between 200 °C and 600 °C. There is only a small weight loss due to adsorbed water or formation of gases before 200 °C. This indicates that the ways used to remove the surfactant during the synthesis procedure are efficient.

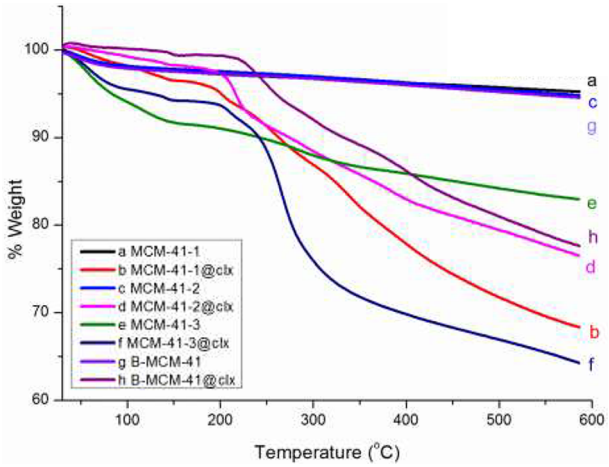

Figure 4. % Weight loss of a) MCM-41-1, b) MCM-41-1@Clx, c) MCM-41-2, d) MCM-41-2@Clx, e) MCM-41-3, f) MCM-41-3@Clx, g) B-MCM-41, h) B-MCM-41@Clx.

In Figure 5 the FTIR spectra of MCM-41 and celecoxib loaded in ethanol and hexane samples are given. Comparing the FTIR spectra of MCM-41 samples (Figures 5A-5D), all of them may seem similar. All MCM-41 samples showed wide adsorption bands in the range of 3750–3000 cm^{-1}. This indicates –OH stretching due to silanol groups in the MCM-41 and adsorbed water. There is a small peak at 2900 cm^{-1}. According to Song et al.,[26] this peak corresponds to –CH stretching of CH_2 or CH_3, which may be due to surfactants that were not removed by calcination or acid extraction. Due to this remaining surfactant in the MCM-41 samples, the peak at 2900 cm^{-1} may be seen.

O–H bending can be seen at 1600 cm^{-1}. This small peak is due to molecular water adsorbed on the silica surface. The surface of MCM-41 is covered with silanol groups and these are water adsorption sites. While the sharper band at around 1100 cm^{-1} is attributed to Si–O–Si asymmetric stretching, the band at around 950 cm^{-1} could be assigned to Si–OH stretching due to silanol groups on the surface. It can be seen that the Si–OH stretching band at 950 cm^{-1} is present in MCM-41-1 (Figure 5A), not present in the calcined samples (MCM-41-2) (Figure 5B), present in MCM-41-3 (Figure 5C), and not present in B-MCM-41 (Figure 5D). Elevated temperature may damage these silanol groups. The peak attributed to O–H bending due to silanol groups on the surface was seen at around 750 cm^{-1}.[30] Celecoxib shows a double sharp peak at 3321 and 3243 cm^{-1} indicating NH_2 stretching in the range of 3200 and 3500 cm^{-1}. While single peaks in the range of 1500 and 1600 cm^{-1} indicate N–H stretching, peaks in the range of 1150 and 1350 cm^{-1} show the presence of

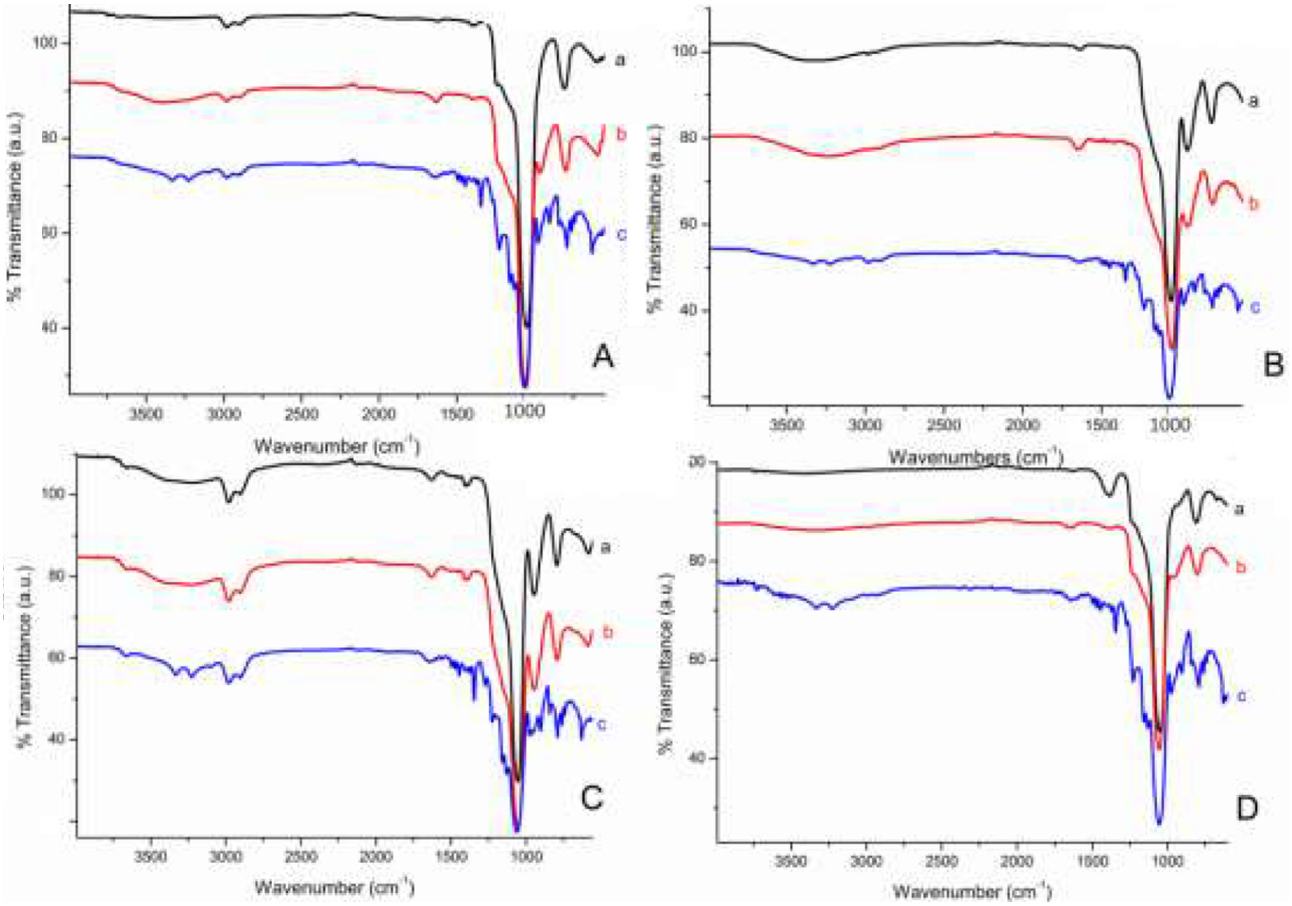

Figure 5. FTIR spectra of A) MCM-41-1 (a) MCM41-1, b) MCM41-1@Clx$_{hex}$ (celecoxib loaded into MCM41 in hexane), c) MCM41-1@Clx$_{eth}$ (celecoxib loaded into MCM41 in ethanol), B) MCM-41-2, (a) MCM41-2, b) MCM41-2@Clx$_{hex}$ (celecoxib loaded into MCM41 in hexane), c) MCM41-2@Clx$_{eth}$ (celecoxib loaded into MCM41 in ethanol), C) MCM-41-3, (a) MCM41-3, b) MCM41-3@Clx$_{hex}$ (celecoxib loaded into MCM41 in hexane), c) MCM41-3@Clx$_{eth}$ (celecoxib loaded into MCM41 in ethanol), D) B-MCM-41, (a) B-MCM41, b) B-MCM41@Clx$_{hex}$ (celecoxib loaded into MCM41 in hexane), c) B-MCM41@Clx$_{eth}$ (celecoxib loaded into MCM41 in ethanol).

sulfonyl groups of sulfonamide in celecoxib.[31] In the comparison of the mixture of MCM-41 and ethanol with MCM-41, there is no specific difference. When the FTIR spectra of MCM-41 samples loaded in hexane were investigated, characteristic peaks of celecoxib that indicate NH_2, N–H, and S=O stretching can be seen. This shows that the drug did not dissolve and was adsorbed mostly on the outer pores on the surface of the MCM-41 samples in hexane, and characteristic peaks of drug were seen easily in the surface characterization by the FTIR spectrum. However, drug molecules that loaded in the inner pores of MCM-41 in ethanol cannot be seen in the FTIR spectrum.

The aim of TEM analysis is to investigate the details of MCM-41 silica particle structure before and after celecoxib loading. In all the reports and studies about MCM-41, it has been stated that MCM-41 has hexagonal arrays of uniform, regularly ordered, two-dimensional cylindrical mesopores. The TEM images of MCM-41 silica nanoparticles that can be seen in the images in Figure 6 prove this statement.[32] According to TEM images, MCM-41-1 (Figure 6A) silica nanoparticles are spherical. They seem to have a diameter of about

30 nm before being loaded with celecoxib and a well-ordered hexagonal array of pores. However, after the drug loading process, the diameters of MCM-41-1 particles increased to 40 nm. Adsorption of the celecoxib drug molecules into the pores and channels of MCM-41 and surface of the carrier particles may increase pore volumes and particle diameter.

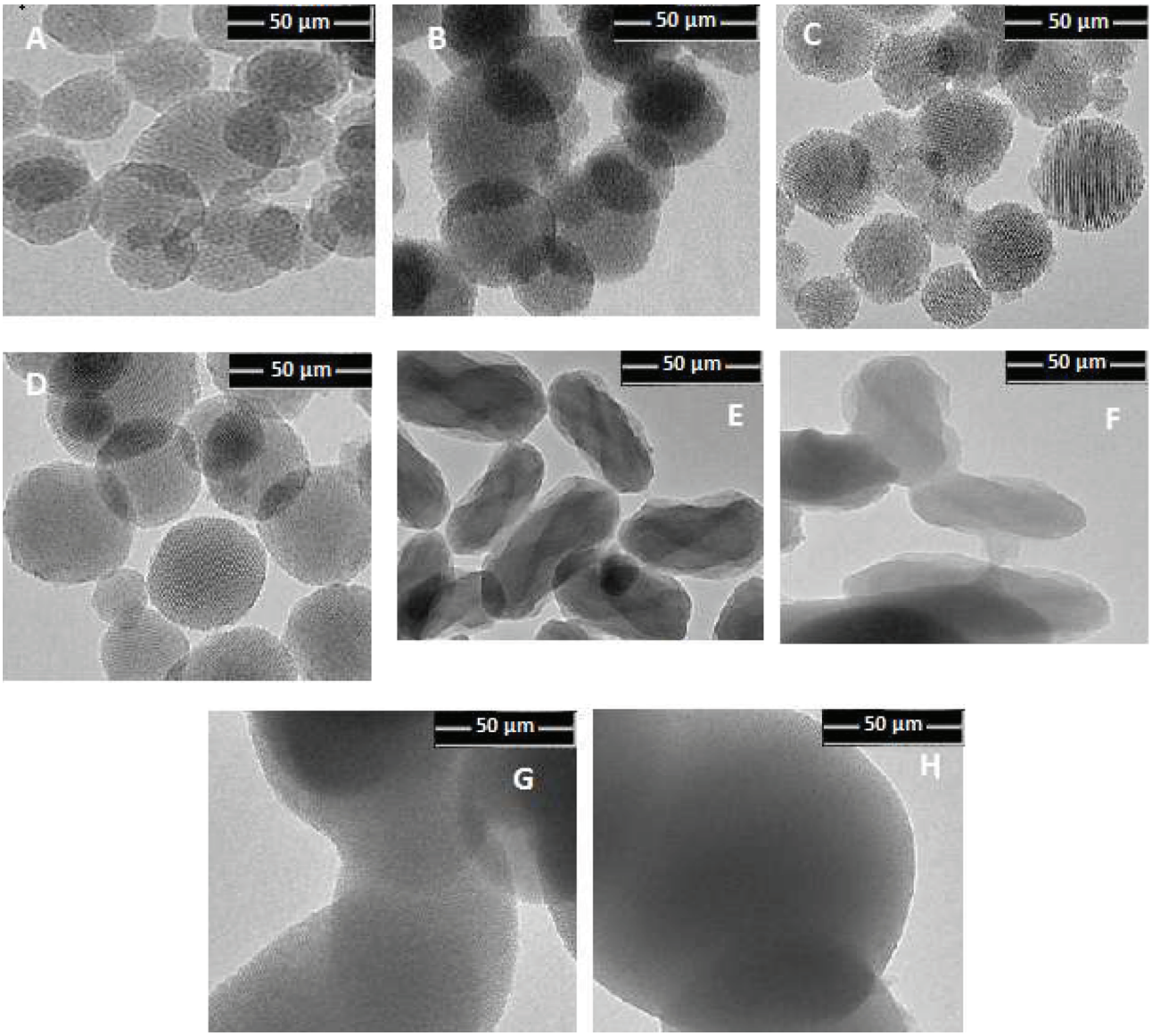

Figure 6. TEM images of A) MCM-41-1, B) MCM-41-1@Clx in ethanol C) MCM-41-2, D) MCM-41-2@Clx in ethanol E) MCM-41-3, F) MCM-41-3@Clx in ethanol, G) B-MCM-41, H) B-MCM-41@Clx in ethanol.

TEM images reveal that the MCM-41-1 (Figure 6A) samples preserve the hexagonal mesoporous structure after drug loading and it can be seen that samples that were calcined show a more ordered array of hexagonal pores compared with MCM-41-1. Elevated temperature probably enhanced the porous structure of the silica and resulted in highly ordered hexagonal pores and a honeycomb structure in TEM images. After drug loading, they also still exhibited ordered pores (Figures 6B-6D). MCM-41-3 samples are different than other MCM-41 samples

in many aspects as can be seen in Figure 6E. Firstly, these particles are rod-shaped. After drug loading, they preserved this morphology (Figure 6F). In the synthesis procedure of MCM-41-3, a slightly high concentration of CTAB probably results in the formation of larger particle size and different morphology. Secondly, in TEM images, pores and channels could not be seen easily before drug loading. Finally, MCM-41-3 silica particles have larger diameters than MCM-41-1 and MCM-41-2 do (Figures 6A and 6C). The MCM-41 sample with the largest diameter is borosilicate. The diameter of one particle is about 400 nm. As shown in Figure 6G, they are spherical. The particles of B-MCM-41 have an ordered array of pores and channels that can be seen easily in TEM images. After drug loading, these pores and channels were probably filled with drug molecules and could not be seen easily in TEM images (Figure 6H).

2.2. Celecoxib loading

According to the amounts of drug loaded onto supports (Table), it can be seen that morphology and particle diameter do not affect the drug loading capacity of MCM-41 silica particles. There are no significant differences in the amount of loaded drug to MCM-41-1, MCM-41-2 silica particles that are spherical with smaller pore diameter, MCM-41-3 with rod shape morphology, and B-MCM-41 that are spherical with larger diameter. It can be seen that the highest amount of celecoxib was not held by the MCM-41-1 particles with the largest pore volume, and MCM-41-1 particles that do not have the largest pore volume held the highest amount of celecoxib. Pore volumes of samples were decreased after drug loading. This proves the loading of drug molecules into the pores of samples. Moreover, the borosilicate sample held the lowest amount of drug, which can be explained by its highly negative surface. Physical adsorption of a poorly soluble drug to a support is more favorable in enhancing drug dissolution because this is a reversible process. Generally, hydrogen bonding and electrostatic interactions are the forms of the physical adsorption between drug molecules and mesoporous silica.[13] In the boron-doped form of MCM-41, the surface is largely covered with –OH groups, making the surface very negatively charged, and the hydrogen bonds and electrostatic attractions are expected to increase the strength of drug and support interactions. Nevertheless, the amount of drug deposited in B-MCM-41 in both the ethanol and hexane solvent systems is not as high as expected. Further, the pore volume of bare borosilicate is not too small, 1.203 g/cm^3, which is the second largest volume in the four samples. The reason for loading a low amount of drug would be the disorder of pores in borosilicate; in the TEM picture the pores cannot be identified clearly (Figures 6G and 6H).

Solvent polarity used in drug adsorption involving a mesoporous silica support is a very important factor in poor water soluble drug loading.[13,33] In this study, our aim was to find the optimum conditions to increase drug loading capacity to a silica support. Therefore, we compared the loading capacities of the drug in ethanol and hexane. While MCM-41 nanoparticles that were loaded with celecoxib in ethanol held 25.95% drug at maximum, this value increased to 29.51% in MCM-4-1 by using hexane in the loading process. This trend is the same and insignificant for the others: e.g., MCM-41-2 and MCM-41-3 have an increased amount of drug loaded in ethanol and hexane from 20.95% to 22.92% and 25.21% to 25.58%, respectively. For these two supports the net negative surface charges are not very big numbers; they are close to neutral values (zeta potential value of MCM-41-2 is –2.94 mV and –2.55 mV for MCM-41-3). Solvent polarity changes have a considerable effect on the drug loading capacity of the boron-containing sample, which has very high net negative surface charges (zeta potential value is –31.7 mV), and hexane use during the loading process increased the amount of drug loaded from 17.57% with ethanol use to 23.89%. These results proved that there are competitive adsorptions with polar solvent and hydrophobic drug molecules and the silica surface; however, hexane shows no polarity

with any competition and increases the amount of drug loading. To understand the different behavior of solvent, the solubility parameter (δ) of the solvents, which denotes the polarities of solvents, may be helpful for the discussion.[34] Generally, higher solubility parameters mean higher polarity of solvents. In terms of the intermolecular interactions, there are several type of parameters grouped into the solubility parameter, such as dispersion, dipole interaction, and hydrogen-bonding interaction (Hansen parameter).[35] The proton acceptor solubility parameter of hexane is zero, while this parameter for ethanol is 19.4 and it is very high number for water (42.3). Hexane has a lower solubility parameter (7.24) than ethanol (12.92). The celecoxib molecule has ammine and trifluoromethyl groups for possible hydrogen bonding. Therefore, it has high affinity with ethanol and dispersed very well in the pores of silica in less crystalline form, while it has lower affinity to hexane due to the lower proton acceptor value of hexane, and the interaction between drug molecules and silanol groups of MCM-41 type of mesoporous silica is stronger, which results in adsorption of drug into the pores of silica in high amounts but in crystalline form, without very good dispersion. In conclusion, ethanol is a better solvent than hexane for drug transfer into the pores of a support in amorphous state.

2.3. Celecoxib release

Dissolution experiments were conducted for all celecoxib loaded samples and Celebrex, which is the commercial form of the drug, by measuring the concentrations of drug released to aqueous solution with UV-Vis spectroscopy and completed within 30 min, 1 h, 2 h, 4 h, and 6 h. Figure 7 indicate the % cumulative amount of celecoxib released to the phosphate buffer (pH 7.4) solution from 1 g of MCM-41 loaded with celecoxib in ethanol (Figure 7A) and in hexane (Figure 7B) within the first 6 h. Based on the results, it can be said that the release rate and dissolution of the celecoxib were enhanced by using MCM-41 silica nanoparticles, because the amounts of Celebrex were lower in comparison with both ethanol- and hexane-loaded samples. Between ethanol- and hexane-loaded samples, the ethanol-loaded form of celecoxib supported MCM-41 mesoporous silica has a higher amount because of the higher solubility of the amorphous form of the drug. Generally, for poorly water-soluble drugs better dissolution is preferred for the noncrystalline and amorphous form due to the weaker binding energy.[22] Figure 2 compares the crystallinity of the drug loaded in ethanol and hexane by showing the powder XRD patterns in a wide angle range.

For poorly soluble drugs, physical adsorption such as hydrogen bonding and electrostatic and hydrophobic interaction is more favorable to enhance dissolution. The dissolution behavior of the drug is reversible in confinement into pores of mesoporous silica and release. In both forms of samples prepared in ethanol and hexane, the borosilicate samples have higher dissolution. High net negative surface charges of borosilicate reduce the support and drug molecule interaction during loading and in the release process this weaker interaction may help transfer of drug molecules to release medium, increasing the solubility of the drug. Other important effects on drug solubility are the particle size of the support and dispersancy of drug molecules in pores: MCM-41-1 and MCM-41-2 have lower particle sizes than MCM-41-3 and smaller particle sized samples have faster release than larger ones. It takes less time for drug molecules in smaller mesoporous spheres to diffuse into release fluid.[14] Xu et al. explained that the pore mouth amount might be the reason: smaller spheres possessed a larger external surface, with more mesoporous pore mouths on the external surface. In addition, the drug release process is mainly a diffusion-controlled process. Once the release fluid penetrated into mesopores, the drug molecules would dissolve and be diffused out from the mesopores along with the solvent-filled pore channels. The drug molecules adsorbed in smaller mesoporous spheres would have more chance to escape from mesoporous materials and diffuse into release fluid. Therefore, the release would take less time than in larger spheres. In our release experiments, we observed that larger particle size in the support caused the lowest cumulative amount of drug;

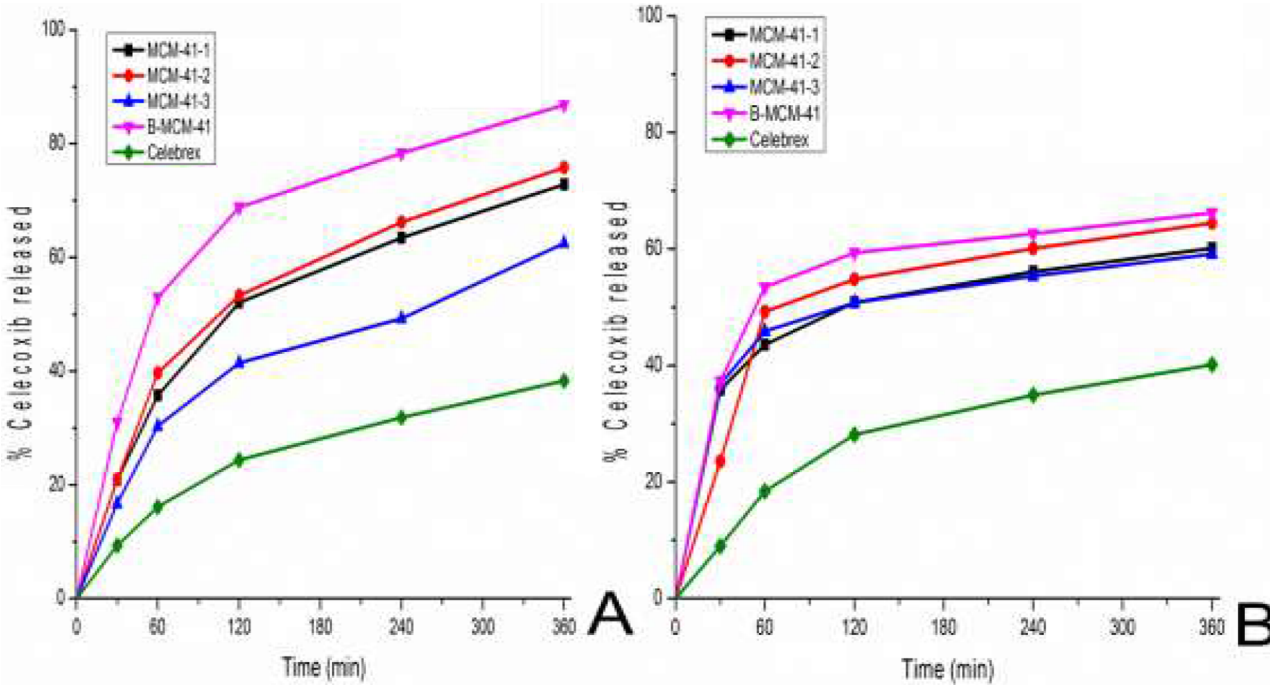

Figure 7. Amount of celecoxib released from 1 g of celecoxib loaded to MCM-41 in ethanol (A) within 6 h and (B) celecoxib loaded to MCM-41 in hexane.

for example, cumulative release percentages in the first 6 h release for MCM-41-3 (nearly 500 nm particle size) has 62.48% in ethanol-loaded form and 59.12% in hexane-loaded form. These numbers are 72.83% in the ethanol-loaded form of MCM-41-1 (less than 50 nm particle size) and 60.11% in the hexane-loaded form and 75.82% for the ethanol-loaded form of MCM-41-2 (more than 100 nm particle size) and 64.44% for the hexane-loaded form of it. For the same morphology of supports the pore size and pore volume are also important factors affecting the release rate of drug. Larger pores have less diffusion resistance due to the spacious pore channels and the drugs move more easily into the dissolution medium.[23] For example, MCM-41-1 (1.438 nm pore diameter and 1.146 $cm^3\ g^{-1}$ pore volume) has lower pore diameter and pore volume than MCM-41-2 (2.487 nm pore diameter and 2.087 $cm^3\ g^{-1}$ pore volume). Figure 7 shows that the release profiles of MCM-41-2 were above and have higher release amount of drug than MCM-41-1 in ethanol- and hexane-loaded samples.

Drug molecules adsorbed on the outer pores of MCM-41 move firstly when the dissolution medium is introduced. However, influx of dissolution medium to inner pores needs a longer duration and these drug molecules are released slowly. On the other hand, during the loading process, drug molecules firstly fill the outer pores and move to the inner arrays in MCM-41 later. Loading and release processes are reversible due to this effect. MCM-41 samples holding lower amounts of celecoxib keep it in the outer pores and release it easily; however, release of the higher amount of celecoxib molecules from MCM-41 takes longer and release does not occur easily.[13] In the comparison between ethanol and hexane, for example for borosilicate, the B-MCM-41 sample, it can be observed that samples loaded with drug in ethanol held lower amounts of drug molecules and release was 86.78% at its maximum; however, samples loaded with celecoxib in hexane held higher amounts of drug and released 66.22% in weight of drug in the first 6 h, which is a lower cumulative release amount than for ethanol-loaded samples. Another observation is the difference between the release amount of drug loaded in ethanol and hexane solvents in the first 30 min. While 20.85% of the celecoxib was released from MCM-41-1

in the first 30 min during the release experiments with samples loaded in ethanol, 35.84% of the celecoxib was released from the samples loaded in hexane. In comparison of these data with recent literature data, it can be seen that this is a lower amount of celecoxib release from mesoporous support. For example, when celecoxib was loaded in ethanol to fibrous mesoporous carbon support whose pore diameters were 4.4–7.0 nm, the amount of drug loaded was higher than in this report (0.599 g/g, drug weight/carrier weight) and it was released faster (more than 70%) in the first 30 min.[22] In addition, Wang and colleagues loaded 20%–30% (by wt) celecoxib into 3D face-centered mesoporous silica with higher pore size (16.0, 6.9, and 3.7 nm) by solvent deposition method in methanol and observed two-stage release in an in vitro drug release experiment: burst release (0–10 min) and prolonged release (10–60 min). The cumulative release of celecoxib from support was 63% (16.0 nm), 46% (6.9 nm), and 58% (3.7 nm) in the first 30 min; pore size values are written in parentheses, proving uniform drug loading and pore size are both very important in enhancing the dissolution properties of poorly water-soluble drugs.[23]

A comparison of the release behavior of ethanol- and hexane-loaded samples indicates that celecoxib's solubility was enhanced by using ethanol during the loading process because drug molecules were dispersed in the inner pores of MCM-41 support in amorphous form. After the influx of solvent to pores, drug molecules were removed from the surface of pores very easily. By this way, the amount of celecoxib release was increased in aqueous solution. However, when hexane solution was used in the loading process due to the lower solubility parameter of hexane the drug molecules were deposited inside the pores of silica supports in preserved crystalline form, which can be observed in the powder XRD pattern (Figure 2). As a result, the quantities of drug analyzed in aqueous solution in release experiments were lower in all hexane-loaded samples than in ethanol-loaded samples.

In conclusion, the amounts of celecoxib loaded into MCM-41 supports with different particle diameters, pore volumes, and net surface charges (by adding boron to mesoporous silica) while using a nonpolar solvent were increased significantly. Moreover, the release of celecoxib molecules was highly improved compared to its commercial drug capsule, Celebrex, by using MCM-41 particles as carrier. The results showed that celecoxib loaded in hexane was in crystalline form and had higher amounts in all samples regardless of morphology than ethanol, which in celecoxib was in noncrystalline state. MCM-41-1 has the highest amount in loading (26% celecoxib in silica by wt/wt loaded ethanol and 30% loaded hexane) and has the lowest particle size: less than 50 nm diameter spherical particles. The release trends of all silica materials drug loaded in ethanol and hexane were the same: the ethanol-loaded samples released more celecoxib in the first 6 h than hexane-loaded samples and between silica samples the lowest amounts of release were observed in particles with larger dimensions. Furthermore, the highest amount of release was observed in boron-doped samples (87% in ethanol loaded and 66% in hexane loaded). These results confirm the potential of silica supports as drug delivery carriers for low water solubility drugs and the morphology of support, surface functionalization, and solubility parameter of solvent used in the loading process must be optimized in order to enhance the dissolution of poorly water-soluble drugs.

3. Experimental

3.1. Materials and chemical reagents

Hexadecyltrimethylammonium bromide (CTAB) was purchased from Fluka and tetraethyl orthosilicate (TEOS, $(C_2H_5O)_4Si$, M_W = 208.33 g/mol) was purchased from Aldrich. Celecoxib (Pfizer, Celebrex, 200 mg), 37% hydrochloric acid (HCl), NaOH, methanol, ethanol, hexane, boric acid (H_3BO_3), ammonia, and acetone were

purchased from Sigma-Aldrich. In addition, KH_2PO_4 was purchased from Merck, while K_2HPO_4 was obtained from Riedel-Haën. All of the chemical reagents were used without further purification. Deionized water was used during the experiments.

3.2. Synthesis of MCM-41 particles

With the synthesis procedure described by Zheng et al., 0.75 g of CTAB was dissolved in 360 mL of deionized water.[36] Next 2 mL of 2 M NaOH solution was added to the CTAB solution and temperature was increased to 80 °C. Then 3.75 mL of TEOS, which is a source of silica, was added to the mixture under stirring drop by drop. This mixture was stirred for 2 h at 80 °C. After the white precipitate formed in 2 h, it was filtered with filter papers, washed with deionized water, and dried at 50 °C overnight in an oven. When the dried sample was obtained, 1 g of the dried silica nanoparticles was taken for acid extraction and mixed with methanol and 37% HCl solution prepared with 100 mL of methanol and 1 mL of HCl. The mixture was mixed at 60 °C for 6 h, filtered, and washed with deionized water. It was dried at 50 °C overnight in the oven. By this way, the surfactant was removed and the silica network of the MCM-41-1 was obtained. As an alternative method to remove the surfactant by acid extraction, calcination was used. White precipitate obtained in the first step was placed in a muffle oven inside a crucible. The ramp rate was 1 °C min^{-1}. To remove the adsorbed water, after the temperature reached 160 °C, the sample was heated at this temperature for 2 h. Then the temperature was increased to 550 °C and the sample was kept at this temperature for 6 h. With this purification technique, we obtained MCM-41-2. For the synthesis of larger particle size MCM-41 (nearly 500 nm), 2 g of CTAB was dissolved in 480 mL of distilled water and 7 mL of 2 M NaOH was added under stirring. The solution was heated up to 80 °C and mixed for 30 min. After 10 mL of TEOS was added to the mixture drop by drop, it was mixed for 2 h at 80 °C. The white precipitate, formed in 2 h, was filtered, washed with deionized water, and dried at 50 °C overnight in the furnace. After it was dried, acid extraction was performed in order to remove the surfactant. Then 1 g of MCM-41-3 sample was added to 100 mL of ethanol and 1 mL of 37% HCl and mixed at 60 °C for 6 h. The sample was dried at room temperature again. By this synthesis procedure, larger particle size MCM-41 silica nanoparticles (500 nm), labeled MCM-41-3, were obtained.

For the synthesis of borosilicate, as described by Zhang et al., 0.64 g of CTAB was dissolved in 32 mL of deionized water. Then 10 mL of 25% NH_3 solution, 14.5 mL of acetone, and 0.155 g of boric acid were added.[37] The solution was mixed for 20 min. After 2.8 mL of TEOS was added, the solution was mixed for 2 h. The white precipitate was filtered, washed with deionized water, and dried in a furnace at 50 °C overnight. Then it was heated at 160 °C for 2 h. The following calcination was done at 550 °C for 6 h and B-MCM-41 was obtained.

3.3. Celecoxib loading

For loading of celecoxib:MCM-41 sample in 1:1 ratio by weight, 0.1 g of MCM-41 and 0.1 g of celecoxib were mixed in 50.0 mL of ethanol for 48 h at ambient temperature with stirring. The suspension was centrifuged and filtered to obtain the sample as precipitate. The celecoxib-loaded silica sample was washed with ethanol and dried at ambient temperature. The same experiments were repeated in hexane. UV analyses were used for quantitative determination of celecoxib. A CARY 5000 UV-VIS-NIR Spectrophotometer was used at a wavelength of 254 nm. The degree of drug loading was determined by extracting drug samples with ethanol under stirring and ultrasonic treatments followed by filtration and then UV analysis. All samples' drug concentrations were determined five times by using the Beer–Lambert law to plot the calibration curve; then the mean value

was calculated. The degree of drug loading was calculated according to the following equation:

$$\text{Degree of drug loading} = \frac{\text{Weight of celecoxib in sample}}{\text{Weight of carrier in sample}}$$

3.4. Celecoxib release

Phosphate buffer solution (PBS) of pH 7.4[21] was prepared for the release experiments. For this purpose, two different phosphate salts were used: K_2HPO_4 and KH_2PO_4. In 1 L of deionized water were dissolved 13.97 g of K_2HPO_4 and 2.69 g of KH_2PO_4. The pH of the prepared solution was adjusted to 7.4 to simulate the pH of the intestine. Then 0.5 g MCM-41 samples loaded with celecoxib were added to 50 mL of PBS. Each of the prepared solutions was mixed at 37 °C in order to simulate the body temperature. The amount of celecoxib released from the silica particles was calculated according to the concentration change within 6 h. The concentration measurements were completed within 30 min, 1 h, 2 h, 4 h, and 6 h.

3.5. Characterization

Powder XRD patterns of the samples were recorded under ambient conditions at 0.9–8° and 10–90° (2θ) with a resolution of 0.05° by using a Rigaku X-ray Diffractometer with a Miniflex goniometer operated at 30 kV and 15 mA. The source of the X-ray radiation was Cu Kα (λ = 1.54 Å). The scanning mode was continuous scanning. The samples were examined with a CHNS-932 (LECO) elemental analyzer to obtain the percentages of carbon within each sample. The carbon measurements were performed twice to obtain adequate results. The thermogravimetric analysis was conducted using a PerkinElmer Thermogravimetric Analyzer. The measurements were made under air at temperatures between 30 and 600 °C with a heating rate of 10 °C min^{-1}. In the IR spectra of the samples, a Bruker IFS 66/S ATR spectrometer was used in the range of 500 and 4000 cm^{-1}. Each sample was characterized before and after the loading of celecoxib. The N_2 adsorption–desorption measurements were examined with a Quantachrome Autosorb-6. Before the measurement, each sample with celecoxib was outgassed at 50 °C for 16 h and samples without drug were outgassed at 110 °C for 16 h. The specific surface areas were calculated using the multiple point BET method. The pore size distributions were calculated using desorption branches of the isotherms by the BJH method. For the TEM analysis, a JEOL JEM 2100F STEM and a JEOL JEM 2100F Field Emission Gun were used during the experiments. The pure samples were operated at 80 kV and after functionalization the samples were analyzed at 120 kV. Before the analysis, MCM-41 silica nanoparticles were dispersed in ethanol in an Elma S 30 H ultrasonic bath for 15 min. Zeta potential measurements were made by using a Malvern Zetasizer Nano ZS instrument. To dissolve the silica nanoparticles in deionized water, they were mixed at 35 °C and ultrasonicated in an Elma S 30 H ultrasonic bath for 30 min.

Acknowledgments

This study was funded by METU BAP-07-02-2012-003 project. In addition, the technical assistance of the Central Laboratory (METU) is acknowledged. The authors would like to express their gratitude to Dr Sreeparna Banerjee from the Biology Department, METU, for her valuable discussions. Dr İrem Erel from the Chemistry Department, METU, is gratefully acknowledged for her help with the zeta potential measurements.

References

1. Kresge, C. T.; Leonowicz, M. E.; Roth, W. J. ; Vartuli, J. C.; Beck, J. S. *Nature* **1992**, *359*, 710–712.
2. Zhao, D.; Huo, Q.; Feng, J.; Chmelka, B. F.; Stucky, G. D. *J. Am. Chem. Soc.* **1998**, *120*, 6024–6036.

3. Kobler, J.; Möller, K.; Bein, T. *ACS Nano* **2008**, *4*, 791–799.
4. Vallet-Regi, M.; Ramil, A.; del Real, R. P.; Perez-Pariente, J. *Chem. Mater.* **2001**, *13*, 308–311.
5. Sevimli, F.; Yilmaz, A. *Microporous and Mesoporous Mater.* **2012**, *158*, 281–291.
6. Garcia, N.; Benito, E.; Guzman, J.; Tiemblo, P.; Morales, V.; Garcia, R. A. *Microporous and Mesoporous Mater.* **2007**, *106*, 129–139.
7. Huh, S.; Wiench, J. W.; Yoo, J.-C.; Pruski, M.; Lin, V. S. Y. *Chem. Mater.* **2003**, *15*, 4247–4256.
8. Yamada, H.; Urata, C.; Ujiie, H.; Yamauchi, Y.; Kuroda, K. *Nanoscale.* **2013**, *5*, 6145–6153.
9. He, Q.; Zhang, J.; Shi, J.; Zhu, Z.; Zhang, L.; Bu, W.; Guo, L.; Chen, Y. *Biomaterials* **2010**, *31*, 1085–1092.
10. Rosenholm J. M..; Peuhu, E.; Eriksson, J. E.; Sahlgren, C.; Linden, M. *Nano Letters* **2009**, *9*, 3308–3311.
11. Stein, A.; Melde, B.; Schroden, R. *Adv. Mater.* **2000**, *12*, 1403–1419.
12. Vallet-Regi, M.; Balas, F.; Colilla, M.; Manzano, M. *Solid State Sci.* **2007**, *9*, 768–776.
13. Xu, W.; Riikonen, J.; Lehto, V. *Int. J. Pharmaceutics* **2013**, *453*, 181–197.
14. Liu, Y.; Sun, C.; Hao, Y.; Jiang, T.; Zheng, L.; Wang, S. *J. Pharm. Pharmaceut. Sci.* **2010**, *13*, 589–606.
15. Paul, S. M.; Mytelka, D. S.; Dunwiddie, C. T.; Persinger, C. C.; Munos, B. H.; Lindborg S. R.; Schacht, A. L. *Nature Rev.* **2010**, *9*, 203–214.
16. Wischke, C.; Schwendeman, S. *Int. J. Pharmaceut.* 2008, *364*, 298–327.
17. Chaudhary, A.; Nagaich, U.; Gulati, N.; Sharma, V.; Khosa V. *J. Adv. Pharm. Edu.* **2012**, *2*, 32–67.
18. Tan, A.; Davey, A.; Presditge, A. *Pharm. Res.* **2011**, *28*, 2273–2287.
19. Jendrossek, V. *Cancer Letters* **2013**, *332*, 313–324.
20. Ligget, L. G.; Zhang, X., Eling, T. E.; Baek, S. J. *Cancer Letters* **2014**, *346*, 217–224.
21. Tan, A.; Simovic, S.; Davey, A.; Rades, T.; Prestidge, C. A. *J. Controll. Rel.* **2009**, *134*, 62–70.
22. Zhao, P.; Jiang, H.; Jiang, T.; Zhi, Z.; Wua, C.; Suna, C.; Zhang, J.; Wang, S. *Eu. J. Pharmaceut. Sci.* **2012**, *45*, 639–647.
23. Zhu, W.; Wan, L.; Zhang, C.; Gao, Y.; Zheng, X.; Jiang, T.; Wang, S. *Mater. Sci. Eng. C.* **2014**, *34*, 78–85.
24. Hoffman, F.; Cornelius, M.; Morell, J.; Froba, M. *Angew. Chem. Int. Ed.* **2006**, *45*, 3216–3251.
25. Kruk, M.; Jaroniec, M. *J. Am. Chem. Soc.* **1997**, *13*, 6267–6273.
26. Song, S.; Hidajat, K.; Kawi, S. *J. Am. Chem. Soc.* **2005**, *21*, 9568–9575.
27. Ravikovitch, P.; Domhnaill, S.; Neimark, A.; Schuth, F.; Ungert, K. *J. Am. Chem. Soc.* **1995**, *11*, 4765–4772.
28. Kaminsky, R. D.; Maglara, E.; Conner, W. *J. Am. Chem. Soc.* **1994**, *10*, 1556–1565.
29. Nieto, A.; Balas, F.; Collilla, M.; Manzano, M.; Vallet-Regi, M. *Microporous and Mesoporous Mater.* **2008**, *116*, 4–13.
30. Primo, F. T.; Fröechlich, P. E. *Acta Farm. Bonaerense* **2005**, *24*, 421–425.
31. Ciesla, U.; Schuth, F.; Wolfgang, J. *Microporous and Mesoporous Mater.* **1999**, *27*, 131–149.
32. Ambrogi, V.; Perioli, L.; Pagano, C.; Latterini, L.; Marmottini, F.; Ricci, M.; Rossi, C. *Microporous and Mesoporous Mater.* **2012**, *147*, 343–349.
33. Martin, A.; Garcia, R. A.; Sen Karaman, D.; Rosenholm, J. M. *J. Mater. Sci.* **2014**, *49*, 1437–1447.
34. Hata, H.; Saeki, S.; Kimura, T.; Sugahara, Y.; Kuroda, K. *Chem. Mater.* **1999**, *11*, 1110–1119.
35. Hansen, C. M. *Hansen Solubility Parameters*; Taylor & Francis: Boca Raton, FL, USA, 2007.
36. Zheng, Q.; Hao, Y.; Ye, P.; Guo, L.; Wu, H.; Guo, Q.; Jiang, J.; Fu, F.; Chen, A. *J. Mater. Chem. B* **2013**, *1*, 1644–1648.
37. Zhang, J.; Liu, M.; Song, C.; Guo, X. *Microporous and Mesoporous Mater.* **2011**, *139*, 31–37.